Journal of Biomedical Optics

BiomedicalOptics.SPIEDigitalLibrary.org

Tissue perfusion rate estimation with compression-based photoacoustic-ultrasound imaging

Min Choi
A. M. James Shapiro
Roger Zemp

SPIE.

Min Choi, A. M. James Shapiro, Roger Zemp, "Tissue perfusion rate estimation with compression-based photoacoustic-ultrasound imaging," *J. Biomed. Opt.* **23**(1), 016010 (2018), doi: 10.1117/1.JBO.23.1.016010.

Tissue perfusion rate estimation with compression-based photoacoustic-ultrasound imaging

Min Choi,[a] A. M. James Shapiro,[b] and Roger Zemp[a,*]
[a]University of Alberta, Department of Electrical and Computer Engineering, Faculty of Engineering, Edmonton, Alberta, Canada
[b]University of Alberta, Alberta Diabetes Institute and Alberta Transplant Institute, Division of General Surgery, Faculty of Medicine and Dentistry, Edmonton, Alberta, Canada

Abstract. Tissue perfusion is essential for transporting blood oxygen and nutrients. Measurement of tissue perfusion rate would have a significant impact in clinical and preclinical arenas. However, there are few techniques to image this important parameter and they typically require contrast agents. A label-free methodology based on tissue compression and imaging with a high-frequency photoacoustic-ultrasound system is introduced for estimating and visualizing tissue perfusion rates. Experiments demonstrate statistically significant differences in depth-resolved perfusion rates in a human subject with various temperature exposure conditions. [DOI: 10.1117/1.JBO.23.1.016010]

Keywords: photoacoustic imaging; ultrasound imaging; perfusion; hemodynamics.

Paper 170338RR received May 25, 2017; accepted for publication Dec. 12, 2017; published online Jan. 18, 2018; corrected Feb. 1, 2018.

1 Introduction

Tissue perfusion can be compromised in a number of disease conditions, including peripheral vascular disease (PVD), sepsis and septic shock, diabetic ulcers, pressure ulcers, and cancer, among others.[1–4] Being able to measure tissue perfusion rates could prove highly impactful to clinical practice. However, few methods exist for doing so. One method for rough assessment of whole limb perfusion is assessment of cutaneous capillary refill time (CRT), which is done by pressing on a nail bed or a finger for 5 s and measuring the time for the pink color to return. However, CRT is devoid of metrics for diagnostic comparisons and is highly variable depending on the patient's size, weight, tissue composition, and much more.[5–8] Therefore, it is used to roughly gauge perfusion abnormality due to hypothermia, PVD, dehydration, and shock. It is not an imaging technique and provides no spatially resolved information about tissue perfusion.

Laser Doppler speckle imaging (e.g., PeriMed), along with other speckle-based imaging such as laser speckle contrast imaging are examples of commercial perfusion-rate tracking system on a peripheral vascular system.[9] However, these systems only measure very superficial blood-flow changes, are not fully quantitative, and provide no depth resolution.[10,11]

Depth-resolved perfusion imaging methods in peripheral vascular system used for preclinical purposes typically require contrast agents and thus limit applicability to screening tasks.[12] Ultrasound imaging is able to measure the rate of perfusion by injecting microbubble contrast agents and destroying them at the imaging site. The reperfusion of these contrast agents is observed and signals are fit to models to estimate spatially resolved reperfusion times.[13–15] While the destruction–reperfusion ultrasound imaging technique is a powerful means of imaging tissue perfusion, some work has shown that the destruction of microbubbles may damage microvascular walls.[16,17]

Other preclinical methods of measuring perfusion rates such as dynamic contrast-enhanced MRI also typically require contrast agents and are not sufficiently low cost or high throughput for widespread screening tasks. These applications have been applied to cerebral perfusion, myocardial perfusion, and cancer imaging, among others.[18,19]

Tissue perfusion has previously been defined as the volume-flow rate of blood exchange per given mass of tissue. In this study, we use a technique similar to ultrasound destruction–reperfusion imaging to estimate the so-called refill rate-associated tissue reperfusion. In the contrast-enhanced ultrasound approach, microbubble contrast agents are injected intravenously and those passing through the imaging plane are subsequently destroyed using an intense ultrasound pulse.[13] The circulating microbubbles will re-establish flow through the imaging area and the signal recovery from the contrast agents is tracked using a recovering exponential model.[13] The time-constant associated with this recovering exponential is the refill rate, and correlates with the tissue perfusion rate. In the present paper, instead of using microbubble contrast destruction–reperfusion methods, we instead use tissue compression and monitor reperfusion of blood using photoacoustic imaging. Similar to the destruction–reperfusion approach, we fit the replenishing blood flow signal to a recovering exponential model to estimate the refill rate. It should be understood that the volume of tissue which is monitored, such as the destruction–reperfusion technique, may not be well defined. However, relative reperfusion maps are still possible and may provide valuable data, which correlate with tissue perfusion.

Photoacoustic imaging is a preclinical technology that enables a label-free method of visualizing various chromophores in the body, which includes but not limited to, oxy- and deoxy-hemoglobin, amino acids, and melanin. Being able to locate,

*Address all correspondence to: Roger Zemp, E-mail: rzemp@ualberta.ca

image and differentiate oxy- and deoxy-hemoglobin allow the imaging technique to visualize vascular networks and quantify oxygen saturation within vessels.[20–22] Furthermore, Doppler shift can occur for acoustic signals generated by moving chromophores, which can be used to determine the rate of blood flow.[23–25] Ultrasound Doppler methods have likewise long been used to estimate blood flow velocities in vessels. However, to date no label-free ultrasound or photoacoustic technique has demonstrated the ability to estimate tissue perfusion rates in bulk tissue volumes involving many subresolvable or undetectable vessels.

Our label-free method uses an ultrasound-photoacoustic (US-PA) dual imaging system to measure the perfusion rates in peripheral regions by pressing on the skin surface directly using the imaging transducer head. Due to the high resolution of PA imaging, we are able to detect net signals from tissue microvasculature, even if the vessel networks are not resolvable, allowing us to quantify changes in PA signals during compression and release. We fit the recovering mean photoacoustic signals to a first-order negative exponential model to create spatially resolved images which quantify perfusion rates. Perfusion-rate differences are seen in various cold- and hot-water-bath exposure conditions.

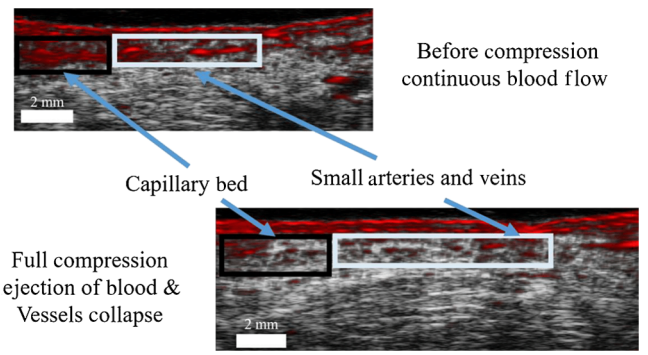

Fig. 1 PA signals of the blood before and during full compression

2 Methods

2.1 *Imaging System*

Changes in capillary beds induced by compressions are imaged using the VEVO LAZR platform (Fujifilm, Visualsonics Inc.), a real-time US-PA dual imaging system. For this experiment, we used a LZ-550 transducer, which has a receive bandwidth of 32 to 55 MHz. Photoacoustic imaging is performed with 805-nm light delivered through a fiber bundle from the VEVO LAZR Optical Parametric Oscillator at the frame rate of 5 Hz. The laser power is 17 mJ/cm^2, which is much lower than the ANSI safety limit of 32 mJ/cm^2 on the human skin and the frame rate is fast enough to detect PA signal changes during reperfusion as CRT in a healthy finger is known to be slightly under 2 s. This wavelength is selected because it is an isosbestic point where the molar extinction coefficient of oxy- and deoxy-hemoglobin is the same. At isosbestic point, the absorption coefficient for oxy- and deoxy-hemoglobin is equal, allowing for unbiased signatures from blood vessels with variable blood oxygenation. As shown in Fig. 1 below, when a soft tissue layer is compressed, blood is excluded from the compression volume, reducing the PA signal in the compressed area. The magnitude of loading rate is not measured nor it is constant. However, the load is measured by a force sensor (iLoad mini™, LoadStar Inc.) to maintain a maximum compressive pressure of 50 kPa for full ejection. The transducer is fixed to a transducer holder mounted on a stage, as shown in Fig. 2(b) for vertical compression. An example of sensing compression force synchronous with tracking the PA signal is shown in Fig. 2(c). Once the transducer is placed on the hand, where the area (20 mm × 5 mm) is marked as shown in Fig. 2(a), it will not change its location for the duration of the experiment. In addition, a custom-made standoff pad (~5 mm) cut from a large ultrasound gel pad (Aquaflex®, Parker Laboratories Inc.) is placed within the transducer head casing to allow uniform pressure distribution along the area of compression. Analogous to US perfusion imaging with contrast agents, the recovering PA signals after compression is released will be fit to a negative exponential model, allowing us to quantify the perfusion rates.

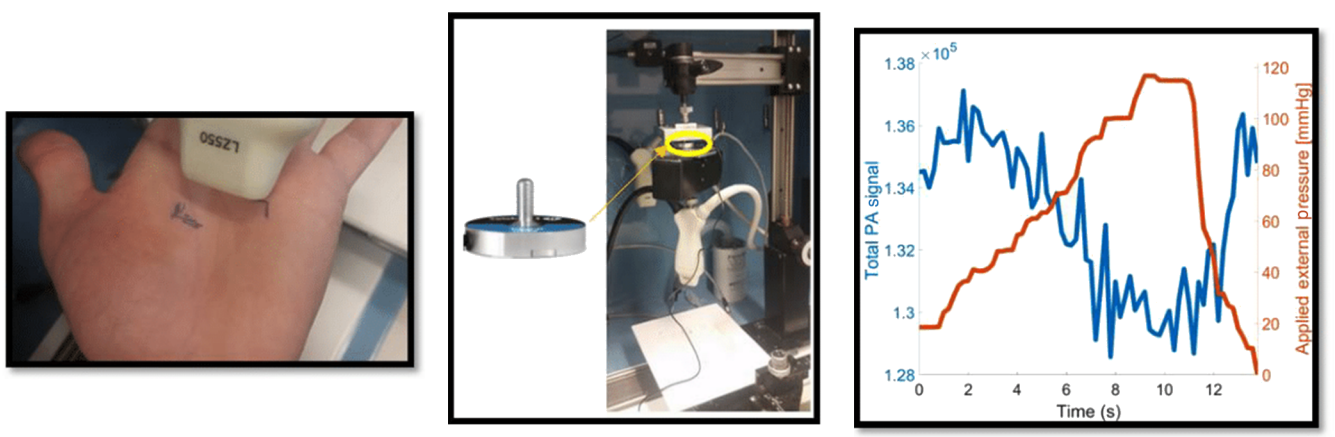

Fig. 2 (a) Location of the transducer on the hand and (b) the transducer fixed on the top along with the force sensor. The transducer and the force sensor are restricted to a vertical movement and (c) an example of PA signal tracking synchronized with pressure sensor reading

2.2 *Human Subject Imaging Study*

To assess the change in perfusion rate, cold- and hot-water immersion tests are performed where the hand of a human subject is submerged in 4°C and 45°C water baths for various durations and the transducer head is used to directly compress on the hand to capture refill of blood vessels. The length of each compression-release (C-R) cycle is up to 10 s long with an interval between each cycle. The length of the interval time is set so that the durations of the C-R cycle and the interval time sum up to 30 s. Up to three cycles are performed. Human subject experiments were conducted in accordance with ethical protocols approved by the University of Alberta Health Research Ethics Board (Pro00007759).

2.3 *Analysis Method*

To demonstrate differences in refill rates of tissues subjected to temperature variations, we imaged a human palm in water immersion baths with different exposure times and temperatures as noted above. Perfusion-rate images were formed using the ultrasound and photoacoustic imaging data using the fitting methods described above.

As shown in Fig. 3(a), on an initial image, a region of interest (ROI), marked by a yellow line, is chosen to define the boundary where the perfusion refill rate estimation will be performed. Within the chosen ROI boundary, a smaller ROI, which is denoted as a "sliding window," shown as a green rectangle in the same figure, is defined. Mean PA signals inside the sliding window at each frame will be directly tracked. Note that the region of tissue associated with a sliding window may change in effective area as the tissue is compressed. We ideally want this sliding window to sample the same tissue volume during each stage of compression. Otherwise, vessels may move in or out of the window during compression, creating unwanted variation in the mean photoacoustic signal. For this reason, we use ultrasound data to track tissue motion to adaptively change the sliding window size to ensure that the same volume of tissue is being measured at each stage of compression.

For this reason, we first separate each image into its respective US and PA components and use ultrasound data to track tissue motion to adaptively change the sliding window size to ensure that the same volume of tissue is being measured at each stage of compression, as shown in Fig. 3(b). Using a robust US strain estimation algorithm AM2D by Rivaz et al.,[26] the RF signal of the B-scan at specific frame and the frame immediately after the chosen frame is processed to estimate both the axial and lateral displacements of the tissue, creating an ultrasound deformation map. The map is applied on the sliding window to create warping.

After PA tracking in a sliding window, started in a specific location is completed, the tracking analysis repeats from the first frame with the sliding window starting from a location bounded by ROI, denoted by a blue arrow in Fig. 3(a). Also, AM2D only needs to run once as deformations are estimated on the entire image area. This process is repeated until the starting location

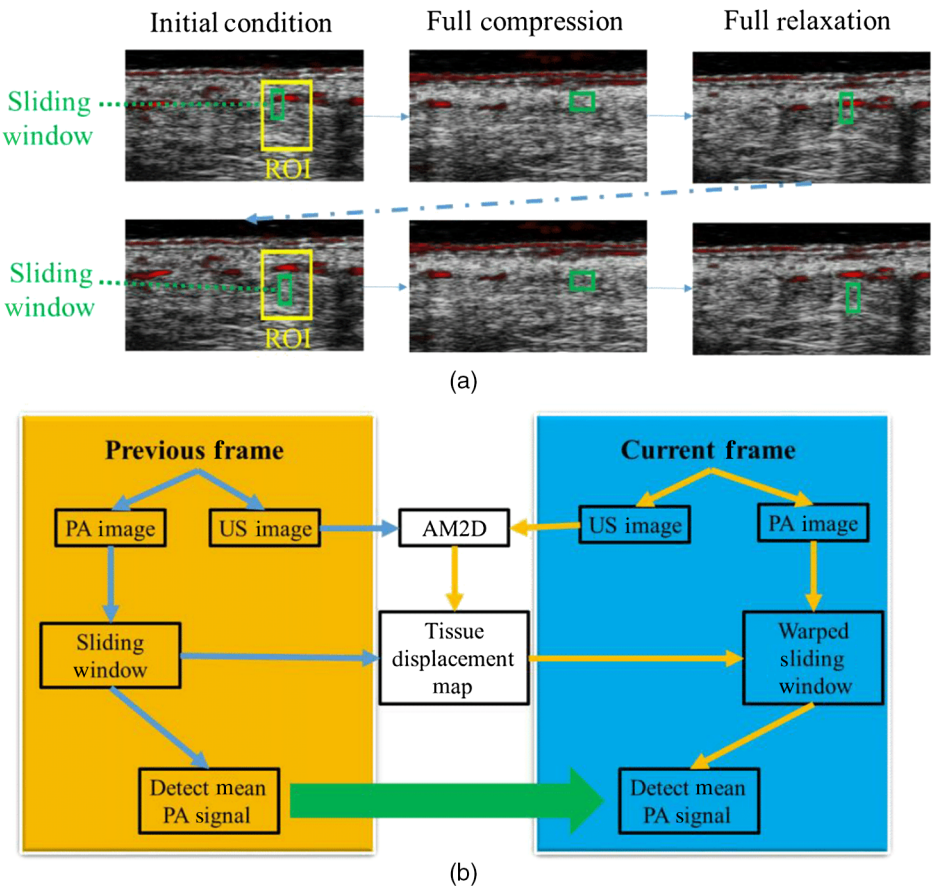

Fig. 3 Schematic of reperfusion rate analysis: (a) placement of the ROI and sliding window in the initial frame and the warping of the sliding window that correlates to the tissue movement. (b) Overview of how PA signals are measured and tracked over multiple frames.

of the sliding window covers the main ROI, the yellow boundary.

During the tracking using MATLAB, large vessels $>\sim 500\ \mu$m (as measured with a 40-dB threshold) were detected and excluded from further PA analysis. This is to prevent flow rates from large vessels skewing the tissue perfusion rates as large vessels have much faster flow rate than arterioles and capillaries and they may be less affected by external temperature changes, which hinder accurate analysis of the perfusion rates of smaller vessel networks.

To estimate the perfusion rates, a negative exponential equation, shown in Eq. (1), is used to model the PA signal recovery after the tissue is released from external loading

$$S = A(1 - e^{-t\rho}) + S_{\min}, \tag{1}$$

where S is the current PA signal strength, A is the PA signal difference between the steady state and the maximum-applied-compression, $S_{\min}$ is the minimum PA signal, which occurs at the maximum compression, and ρ represents the refill rate. The beginning of the release of compression is determined by the ultrasound strain map image sequence. An example of the tracking of the PA signal during tissue movement and the fitting of the obtained data is shown in Fig. 4.

3 Results

To demonstrate differences in reperfusion rates of tissues subjected to temperature variations, we imaged a human palm in water immersion baths with different exposure times and temperatures as noted above. Perfusion-rate images were formed using the ultrasound and photoacoustic imaging data using the fitting methods described above.

The distribution of perfusion rates within the main ROI when the hand is submerged in the cold and hot water baths is shown in Fig. 5. Clear differences in the perfusion-rates are seen between differing temperature exposure conditions as visualized by the red-to-blue colormaps with red and blue colors representing fast and slow refill rates, respectively. Here the size of the main ROI is 6.21-mm wide × 3.25-mm deep, and images in Fig. 5 had a sliding window size of 4.24 mm × 0.78 mm to detect changes in PA signal. To explore how window sizes affect perfusion-rate estimates as larger window for averaging tends to reduce effect of noise, additional window sizes of 2.83 mm × 0.78 mm, 1.41 mm × 0.78 mm, and 0.78 mm × 1.95 mm, respectively, are used and compared in Fig. 6. For 30, 60, and 90 s that the hand was submerged in the 4°C water bath, the mean refill rate constant ranges from 0.28 to 0.38 s^{-1}, 0.29 to 0.34 s^{-1}, and 0.14 to 0.22 s^{-1}, respectively. In contrast,

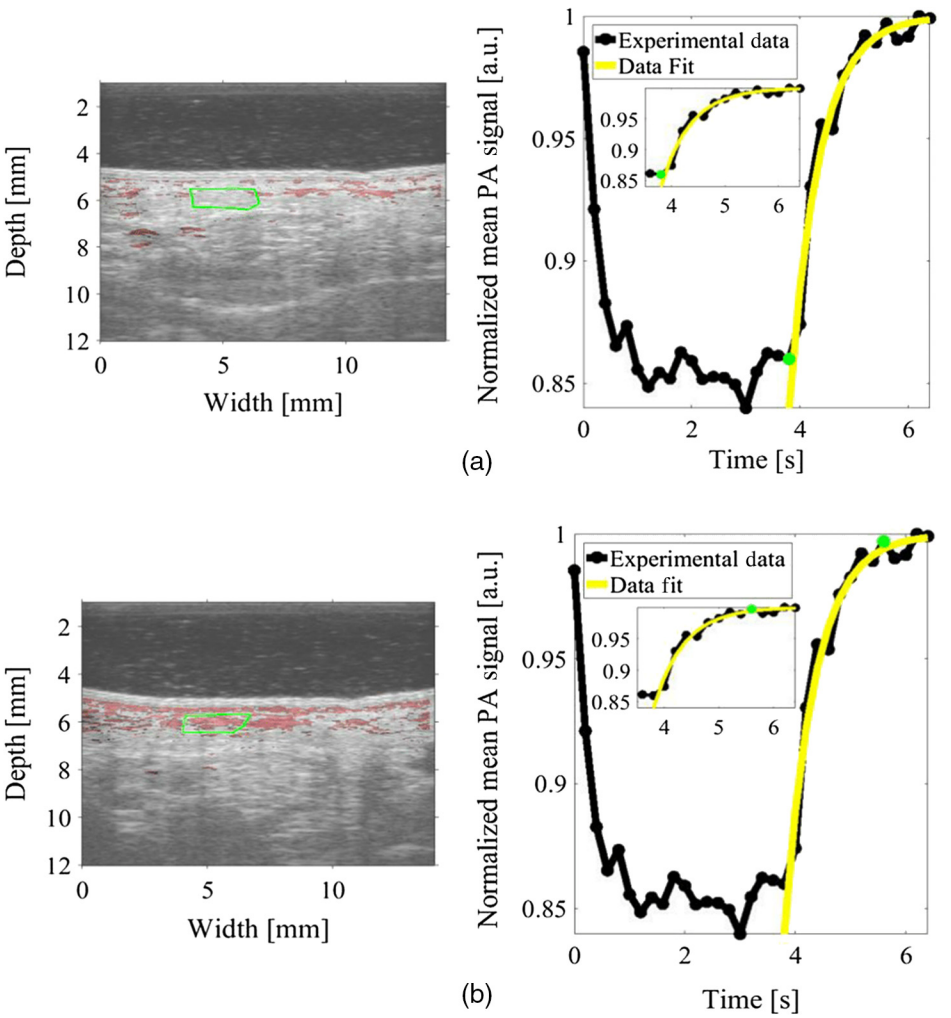

Fig. 4 The transformation of a sliding window (a) during slight relaxation and (b) full relaxation using displacement estimated by AM2D. The small plots within the large plots are magnified version of the large plot.

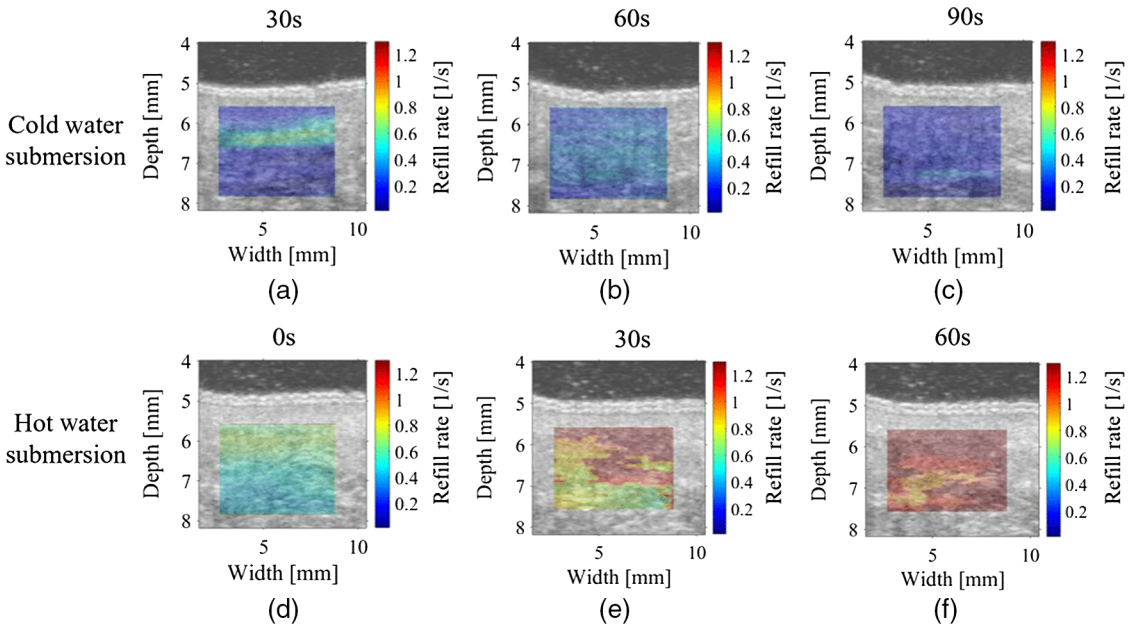

Fig. 5 The refill rate distribution of the left hand of a human subject in the (a)–(c) 4°C water bath for 30, 60, and 90 s, respectively, and (d)–(f) 45°C water bath for 0, 30, and 60 s, respectively. Times shown above each image denote the exposure time at the start of each C-R cycle. The size of sliding window is 4.24-mm wide and 0.78-mm long.

Table 1 The estimated mean refill rates. The submersion time is the duration the hand was submerged in a water bath before the start of the compression.

	Mean refill rate (s – 1)					
Window size depth × length (mm × mm)	Water temp	4°C			45°C		
	Submersion time (s)	30	60	90	0	30	60
4.24 × 0.78		0.31	0.37	0.14	0.59	1.18	1.56
2.83 × 0.78		0.34	0.33	0.18	0.57	0.97	1.26
1.41 × 0.78		0.32	0.29	0.19	0.55	0.91	1.2
0.78 × 1.95		0.5	0.31	0.22	0.56	0.87	1.27

when the hand is submerged in a 45°C water bath for 0, 30, and 60 s, the mean refill rate constant ranges from 0.53 to 0.56 s^{-1}, 0.84 to 1.16 s^{-1}, and 1.15 to 1.59 s^{-1}, respectively, depending on window sizes. The mean refill rates are listed in Table 1. The exposure time shown in Fig. 6 denotes the start time for each C-R cycle. The standard deviation of the perfusion rates varies with window size and is smallest when the sliding window is 1.41 mm × 0.78 mm.

4 Discussion

We have demonstrated a method to image the perfusion rates in superficial tissues using a noninvasive, label-free, and US-PA imaging system. Statistically significant differences using paired *t*-tests were observable ($p < 0.05$) in mean perfusion-rates in multiple cold and hot temperature-exposure conditions. In addition, the distribution of perfusion rates in superficial tissue up to several mm depths can be estimated. Lower frequency probes and higher power light delivery could enable depths of multiple cms in future work.

The ultrasound-photoacoustic system is capable of additional imaging modes, such as color Doppler and power Doppler. In principle, power Doppler could potentially be used to estimate the changes in flow associated with refill after release of compression. However, when tissue is compressed or released, the flow signal from vessels is overwhelmed with the Doppler signal from tissue motion. This takes several seconds to recover, which is too long considering that the capillary refill occurs within a couple of seconds (Fig. 6).

The variance of the perfusion-rate estimates increases with increasing body temperature. This may be due to the fact that fewer data points exist on the recovering exponential fit when the reperfusion rate is high. Errors in displacement estimation impact how a given region of tissue deforms and thus impacts the associated window deformation for analysis. Future work should investigate the impact of errors in this changing window size. Using an imaging system with higher frame rate will improve the temporal resolution of the perfusion rates and will permit faster C-R cycles. Future work should investigate optimal sliding window sizes, optimize for large-vessel rejection, and push limits of depth and frame rate. Furthermore, more careful analysis from larger sets of data should be performed. Reperfusion rate measurements using ultrasound perfusion phantoms and *in vivo* studies involving multiple human subjects must be performed, which may improve data sensitivity and yield more accurate results.

Perfusion-rate estimation method used in this paper deals with photoacoustic signal that are detectable but are spatially unresolvable. The large standard deviation may be due to the low SNR of unresolvable signals. In addition, the hand was not restrained during the measurement and the human subject had to intentionally focus on keeping the hand still. For future works, a laser system with higher power delivery and higher frequency

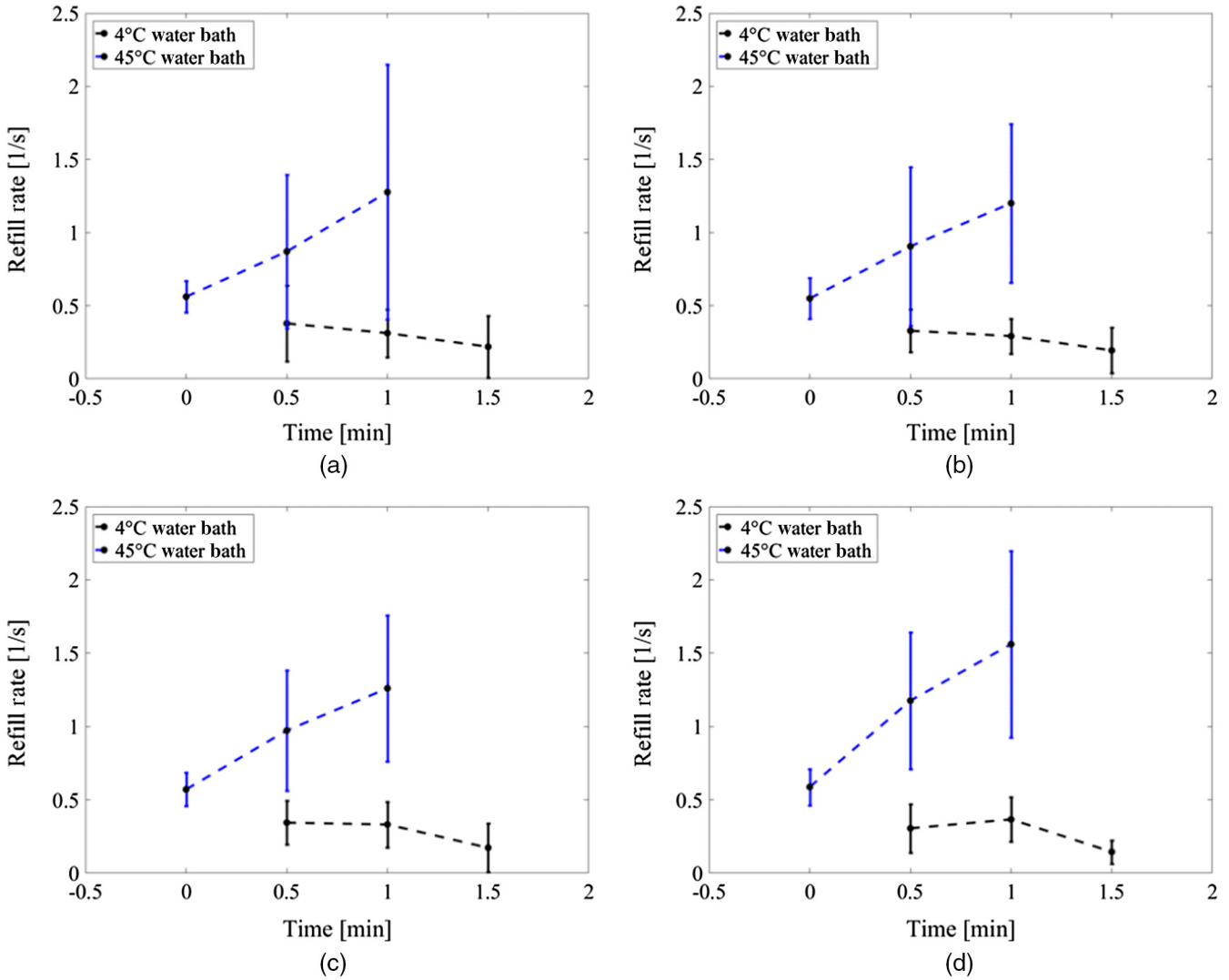

Fig. 6 The average perfusion rates with different sliding window sizes as a function of exposure time in the hot- and cold-water baths. Subfigures are for the following initial sliding window sizes. (a) 4.24 mm × 0.78 mm, (b) 2.83 mm × 0.78 mm, (c) 1.41 mm × 0.78 mm, and (d) 0.83 mm × 1.95 mm.

transducer will allow improved SNR for small vessels, allowing more accurate analysis of perfusion-rate estimation.

As tissue is compressed, both acoustic and optical properties of tissues may be impacted.[27] Applied pressure may also exclude blood, lowering the net absorption, while effective distance to vessels will decrease. Thus compression may alter effective fluence at vessel locations. Currently, the present analysis ignores such effects but future work should aim to better incorporate these effects for more quantitative perfusion-rate estimation.

The negative exponential model for calculating the perfusion rate, ρ, is analogous to the wash-in rate (WIR) of contrast agents used in various contrast-enhanced perfusion imaging techniques. Future work could compare our label-free compression-reperfusion method with contrast-based perfusion imaging techniques. However, it is anticipated that quantitative perfusion rates from our approach may not necessarily match reperfusion rates from contrast-based approaches. For example, the WIR of destruction–reperfusion contrast ultrasound may depend on the thickness of the elevational beam waist, among other considerations. The WIR of our compression-reperfusion PA imaging will largely depend on the size of the compression area and internal pressures may be depth dependent. Future work should investigate these issues and correlate our label-free approach with contrast-enhanced methods.

Label-free perfusion imaging could have a significant role in assessing tissue health in a number of diseases, including diabetes, cancer, etc.[3,17,18] Dynamic contrast-enhanced MRI has show significant potential for discriminating malignant from healthy tissues in a range of cancers including breast cancer and prostate cancer. However, it is expense and the necessity of contrast injections precludes it from widespread screening applications. Our approach is not only label free but potentially high throughput and relatively low cost. Future work should investigate deeper tissues and various cancers and disease models.

Viscoelasticity of the soft tissue may introduce tissue relaxation that can reopen vessels during the compression phase. However, the impact of these effects should be minimal as compression and relaxation are performed on timescales faster than tissue viscoelastic relaxation rates, typically several seconds.[28–30] Future work should investigate the impact of tissue viscoelastic properties on perfusion-rate estimation and account for heterogeneity in tissue mechanical properties.

5 Conclusions

We have demonstrated a label-free imaging method for mapping perfusion rates of tissues using C-R photoacoustic and ultrasound microimaging. Given it is real-time and label-free nature, the approach could have significant value in clinical settings where high-throughput screening is desirable.

Disclosures

The authors have no relevant financial interests in this article and no potential conflicts of interest to disclose. R. Zemp is chief scientific officer and cofounder of illumiSonics Inc., which, however, did not support this work.

Acknowledgments

We gratefully acknowledge funding from NSERC (355544-2008, 375340-2009, STPGP 396444), Terry-Fox Foundation and the Canadian Cancer Society (TFF 019237, TFF 019240, CCS 2011-700718), Alberta Innovates Health Solutions AIHS CRIO Team Award No. 201201154, the Alberta Cancer Research Institute (ACB 23728), the Canada Foundation for Innovation, Leaders Opportunity Fund (18472), Alberta Advanced Education and Technology, Small Equipment Grants Program (URSI09007SEG), and Alberta Ingenuity/Alberta Innovates scholarships for graduate and undergraduate students.

References

1. K. A. Cawcutt and S. G. Peters, "Severe sepsis and septic shock: clinical overview and update on management," *Mayo Clin. Proc.* **89**(11), 1572–1578 (2014).
2. J. Cox, "Predictors of pressure ulcers in adult critical care patients," *Am. J. Crit. Care* **20**(5), 364–375 (2011).
3. A. Satoh et al., "Role of perfusion CT in assessing tumor blood flow and malignancy level of gastric cancer," *Digestive Surg.* **27**(4), 253–260 (2010).
4. G. Russo et al., "Angiogenesis in prostate cancer: onset, progression and imaging," *BJU Int.* **110**(11 C), E794–E808 (2012).
5. M. H. Gorelick, K. N. Shaw, and M. D. Baker, "Effect of ambient temperature on capillary refill in healthy children," *Tech. Rep.* **92**(5), 699–702 (1993).
6. A.-T. Lobos and K. Menon, "A multidisciplinary survey on capillary refill time: Inconsistent performance and interpretation of a common clinical test," *Pediatr. Crit. Care Med.* **9**(4), 386–391 (2008).
7. A. Pickard, W. Karlen, and J. M. Ansermino, "Capillary refill time: is it still a useful clinical sign?" *Anesthesia Analgesia* **113**(1), 120–123 (2011).
8. B. Anderson et al., "Impact of patient and environmental factors on capillary refill time in adults," *Am. J. Emergency Med.* **26**(1), 62–65 (2008).
9. M. Draijer et al., "Review of laser speckle contrast techniques for visualizing tissue perfusion," *Lasers Med. Sci.* **24**(4), 639–651 (2009).
10. V. Rajan, "Influence of tissue optical properties on laser Doppler perfusion imaging, accounting for photon penetration depth and the laser speckle phenomenon," *J. Biomed. Opt.* **13**(2), 024001 (2008).
11. A. Humeau-Heurtier et al., "Relevance of laser doppler and laser speckle techniques for assessing vascular function: State of the art and future trends," *IEEE Trans. Biomed. Eng.* **60**(3), 659–666 (2013).
12. J. R. Lindner et al., "Limb stress-rest perfusion imaging with contrast ultrasound for the assessment of peripheral arterial disease severity," *JACC* **1**(3), 343–350 (2008).
13. D. Cosgrove and N. Lassau, "Imaging of perfusion using ultrasound," *Eur. J. Nucl. Med. Mol. Imaging* **37**(Suppl 1), 65–85 (2010).
14. F. Kiessling, J. Huppert, and M. Palmowski, "Functional and molecular ultrasound imaging: concepts and contrast agents," *Current Med. Chem.* **16**(5), 627–642 (2009).
15. D. Duerschmied et al., "Contrast ultrasound perfusion imaging of lower extremities in peripheral arterial disease: a novel diagnostic method," *Eur. Heart J.* **27**(3), 310–315 (2006).
16. T. Ay et al., "Destruction of contrast microbubbles by ultrasound: effects on myocardial function, coronary perfusion pressure, and microvascular integrity," *Circulation* **104**(4), 461–466 (2001).
17. J. M. Tsutsui, F. Xie, and R. T. Porter, "The use of microbubbles to target drug delivery," *Cardiovasc. Ultrasound* **2**, 23 (2004).
18. F. Kalifa et al., "Models and methods for analyzing DCE-MRI: a review," *Med. Phys.* **41**(12), 124301 (2014).
19. T. S. Koh et al., "Cerebral perfusion mapping using a robust and efficient method for deconvolution analysis of dynamic contrast-enhanced images," *NeuroImage* **32**(2), 643–653 (2006).
20. J. J. Niederhauser et al., "Combined ultrasound and optoacoustic system for real-time high-contrast vascular imaging in vivo," *IEEE Trans. Med. Imaging* **24**(4), 436–440 (2005).
21. S. Hu and L. V. Wang, "Photoacoustic imaging and characterization of the microvasculature," *J. Biomed. Opt.* **15**(1), 011101 (2010).
22. J. Xia, J. Yao, and L. V. Wang, "Photoacoustic tomography: principles and advances," *Electromagn. Waves* **147**, 1–22 (2014).
23. H. Fang, K. Maslov, and L. V. Wang, "Photoacoustic doppler effect from flowing small light-absorbing particles," *Phys. Rev. Lett.* **99**(18), 184501 (2007).
24. J. Yao, "Transverse flow imaging based on photoacoustic Doppler bandwidth broadening," *J. Biomed. Opt.* **15**(2), 021304 (2010).
25. J. Brunker and P. Beard, "Velocity measurements in whole blood using acoustic resolution photoacoustic Doppler," *Biomed. Opt. Express* **7**(7), 2789–2806 (2016).
26. H. Rivaz et al., "Ultrasound elastography: a dynamic programming approach," *IEEE Trans. Med. Imaging* **27**(10), 1373–1377 (2008).
27. E. K. Chan et al., "Effects of compression on soft tissue optical properties," *IEEE J. Sel. Top. Quantum Electron.* **2**(4), 943–950 (1996).
28. A. Tirella, G. Mattei, and A. Ahluwalia, "Strain rate viscoelastic analysis of soft and highly hydrated biomaterials," *J. Biomed. Mater. Res.* **102**(10), 3352–3360 (2014).
29. J. Palacio-Torralba et al., "Quantitative diagnostics of soft tissue through viscoelastic characterization using time-based instrumented palpation," *J. Mechan. Behav. Biomed. Mater.* **41**, 149–160 (2015).
30. H. Zhang, Y. Wang, and M. F. Insana, "Ramp-hold relaxation solutions for the KVFD model applied to soft viscoelastic media," *Meas. Sci. Technol.* **27**(2), 025702 (2016).

Min Choi is pursuing an MSc degree at the University of Alberta, with a focus on using photoacoustic and ultrasound imaging to study the vascular system.

A. M. James Shapiro is a clinician-scientist and professor of surgery at the University of Alberta. He led a clinical team to pioneer the "Edmonton Protocol" islet transplant program which has become internationally known. He has been the recipient of multiple awards, including the Hunterian Medal from the Royal College of Surgeons of England, the Gold Medal in Surgery from the Governor General of Canada, Physician of the Century, and was recently named one of Nature Biotechnology's most remarkable and influential personalities. He was elected fellow of the Royal Society of Canada in 2012. He is a clinical hepatobiliary and pancreatic oncology and transplant surgeon, and also maintains an active immunology/transplant research laboratory. His group is actively researching personalized medicine approaches to pancreatic and other hepatobiliary cancers, with generation of human tumor transplantation in immunodeficient mouse models, using a novel prevascularized subcutaneous implantation site model.

Roger Zemp is a professor of electrical and computer engineering and biomedical engineering at the University of Alberta. He earned his PhD from the University of California, Davis in 2004. He was a postdoctoral fellow in the Optical Imaging Laboratory of Lihong Wang at Texas A&M University and Washington University in St. Louis from 2004 to 2007. He joined the faculty at the University of Alberta in 2007. He has pioneered the development of novel photoacoustic imaging technologies including Photoacoustic Remote Sensing, and developed strategies for photoacoustic molecular imaging. He also has pioneered novel methods of ultrasonic three-dimensional and ultrafast imaging and leads a multidisciplinary team of engineers, biologists, chemists, and clinicians to develop new biomedical imaging strategies for clinical and biological applications.